Bending analysis of smart functionally graded plate using the state-space approach

Niloufar Salmanpour [1a], Jafar Rouzegar [*1], Farhad Abad[2b] and Saeid Lotfian[2c]

[1]*Department of Mechanical Engineering, Shiraz University of Technology, Shiraz, PO Box-71555-313, Iran.*
[2] *Department of Naval Architecture, Ocean and Marine Engineering, University of Strathclyde, Glasgow G4 0LZ, UK.*

(Received April 06, 2023, Revised August 08, 2024, Accepted August 08, 2024)

Abstract. This study uses the state-space approach to study the bending behavior of Levy-type functionally graded (FG) plates sandwiched between two piezoelectric layers. The coupled governing equations are obtained using Hamilton's principle and Maxwell's equation based on the efficient four-variable refined plate theory. The partial differential equations (PDEs) are converted using Levy's solution technique to ordinary differential equations (ODEs). In the context of the state-space method, the higher-order ODEs are simplified to a system of first-order equations and then solved. The results are compared with those reported in available references and those obtained from Abaqus FE simulations, and good agreements between results confirm the accuracy and efficiency of the approach. Also, the effect of different parameters such as power-law index, aspect ratio, type of boundary conditions, thickness-to-side ratio, and piezoelectric thickness are studied.

Keywords: state-space concept; piezoelectric layer; Levy's solution; refined plate theory; bending

1. Introduction

Functionally graded materials (FGM) could be considered special composites when properties change gradually from one layer to another. They have the potential to be designed for a variety of applications, such as biomedical engineering, the renewable energy sector and aerospace industries (Mahamood and Akinlabi 2017). Rahimi *et al.* (2018) investigated the non-linear free vibration of FGM nano-beams using the fractional non-local model. Stempin and Sumelka (2021) extended the space-fractional Timoshenko beam theory to account for non-locality in the bending of FGM beams. Chan *et al.* (2022) presented FGM sandwich cylindrical panels based on the non-local strain gradient theory. Zenkour and Radwan (2020) explored how exponential temperature and moisture concentration impact the bending and buckling behavior of functionally graded plates supported by two-parameter elastic foundations, utilizing a four-variable exponential shear deformation theory. Also, piezoelectric materials are in the spotlight of many researchers because of their properties, such as electromechanical coupling, large power generation, quick response, vacuum compatibility, and the ability to function at low temperatures (Abad *et al.* 2023). These materials are usually attached to the surfaces of plates and shells as actuators and sensors to improve their mechanical properties. Numerous works have been conducted regarding the FG structures with or without piezoelectric layers by employing different solution methods and plate theories (Arefi *et al.* 2019; Guellil *et al.* 2021; Huang and Tahouneh 2021; Kouider *et al.* 2021; Pham *et al.* 2021). Arefi and Soltan Arani (2020) analyzed functionally graded plates with two FG piezoelectric layers at the top and bottom subjected to an electric field using higher-order shear and normal deformation theory. Abbaspour and Arvin (2021) presented buckling analyses of FG graphene platelets micro-plates bonded with two piezoelectric layers. They generated the governing equations using the Kirchhoff plate theory assumptions and the modified couple stress theory and studied the effect of thermal, electrical and mechanical loadings on the buckling of the structure.

The classical plate theory (CPT) is inappropriate for analyzing thick plates, on the other hand, the first-order shear deformation theory (FSDT) cannot fulfil the condition of zero stress on free surfaces and needs a shear correction factor. These limitations led to the development of several higher-order shear deformation theories (HSDTs) (Boukhlif 2019; Zarga 2019; Atmane *et al.* 2021; Belabed *et al.* 2021). However, due to the complexity of the HSDT formulation, researchers have recently developed refined plate theories (RPTs) which improve accuracy and computational efficiency in analyzing FGMs (Menasria *et al.* 2020; Hachemi *et al.* 2021). One efficient but straightforward RPTs is the four-variable refined plate theory which predicts a parabolic variation of transverse shear stresses through the

[a]Ph.D. Student, E-mail: salmanpour_niloufar@yahoo.com
*Corresponding author, Associate Professor,
E-mail: rouzegar@sutech.ac.ir

[b]Ph.D., E-mail: farhad.abad@strath.ac.uk

[c]Ph.D., E-mail: saeid.lotfian@strath.ac.uk

This is a peer-reviewed, accepted manuscript of the following paper: Salmanpour, N., Rouzegar, J., Abad, F., & Lotfian, S. (2024). Bending analysis of smart functionally graded plate using the state-space approach. Steel and Composite Structures, 52(2), 525-541. https://doi.org/10.12989/scs.2024.52.5.525

plate thickness while satisfying the zero-traction condition on the free surfaces. Several researchers have employed this theory for the static and dynamic analysis of FG plate with and without piezoelectric layers (Rouzegar and Abad 2015; Fourn *et al.* 2018; Rouzegar *et al.* 2020).

The state-space approach is an effective analytical method for solving ordinary differential equations. This process reduces the higher-order differential equations to a collection of first-order differential equations, simplifying the solution. Many researchers have used the concept of state-space combined with the well-known Levy's solution to address the different analyses of plate structures. In order to perform buckling, bending, and vibration analysis of thick plates, Thai *et al.* (2013) and Thai and Choi (2013a) used Levy's solution method and the state-space methodology based on an improved shear deformation plate theory. Demirhan and Taskin (2017), (2019) investigated FG plates' bending and free vibration using the four-variable refined plate theory and a Levy-type state-space technique. Liu *et al.* (2022) proposed the state-space approach for free and forced vibration analysis of reinforced concrete beams externally strengthened with fiber-reinforced polymer (FRP) with various boundary conditions. They studied the effect of different parameters and validated their results with those of Abaqus software. Razgordanisharahi *et al.* (2023) developed the state-space method for free vibration analysis of honeycomb sandwich panels and investigated the effect of geometrical parameters on the structure's natural frequencies. The state-space method has also been employed for various analyses of plate structures integrated with piezoelectric elements. To cope with the static analysis of simply supported laminated piezoelectric plates exposed to sinusoidal mechanical and electrical stresses, Lee and Jiang (1996) developed an exact method based on the state-space concept. Huang *et al.* (2020) utilized the state space approach for free vibration, buckling and dynamic impulse response analysis of a multilayered piezoelectric cylinder. Zhou *et al.* (2020) used the state-space approach for static analysis of the laminated curved beam bonded with piezoelectric actuators. Also, to prove the effectiveness of the presented method, they solve several examples of beams with piezoelectric layers. Rouzegar *et al.* (2022) investigated the FG core and two piezoelectric face-sheets with various boundary conditions, applying refined plate theory and using the state-space Levy method.

A review of the available literature has specified that no comprehensive study for bending analysis of FG plates integrated with piezoelectric layers is based on Levy's solution and the state-space approach. In this study, the coupling between the electric potential induced in the piezoelectric layer and the other mechanical variables is considered, while in many studies, the induced voltage is neglected. Hamilton's principle and Maxwell's equation generate the linked governing equations based on the four-variable improved plate theory. A Levy-type solution approach is used to solve the partial differential system of equations. Such a solution converts partial differential equations (PDEs) to ordinary differential equations (ODEs). The state-space approach solves coupled higher-order ODEs by converting them into a system of first-order ODEs. Since the bending analysis of FG plates integrated with two closed-circuit piezoelectric layers exposed to uniformly distributed external loads has not yet been performed, the results are compared with those of the commercial Abaqus package. The effects of various boundary conditions, the power-law index, the aspect ratio, the thickness of the piezoelectric layer, and the thickness of the core layer are all examined in relation to how the structure bends.

In this section, an introduction and a review of the most significant publications related to the subject have been included. The structure of the paper is outlined as follows: Section 2 presents the formulation of the governing equations and the solution method, using the Levy method in conjunction with the state-space approach. Section 3 illustrates the obtained results, provides corresponding discussions, and examines the effects of various boundary conditions, the power-law index, the aspect ratio, and the thickness through three sets of examples. Section 4 offers conclusions and concluding remarks.

2. Theoretical Formulation

2.1 Problem description and assumptions

Fig. 1 shows a schematic view of an FG plate with dimensions a, b, and $2h$ as its length, width, and thickness, respectively which is sandwiched between two piezoelectric layers with a thickness of h_p. It is assumed that the hybrid plate has two opposite simply supported edges at x=0 and x=a while two other edges have arbitrary boundary conditions. The distributed mechanical load $q(x,y)$ is applied to the top face of the structure. Since the main aim of this paper is to investigate the bending behavior of the plate, the loading is considered to be perpendicular to the plate surface.

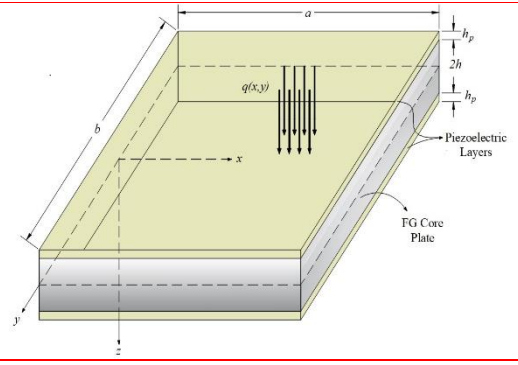

Fig. 1 FG plate subjected to an external distributed load $q(x,y)$ with two piezoelectric layers attached to the top and bottom surfaces.

Effective properties of the FG core plate change according to the rule of mixture

$$E(z) = E_m + (E_c - E_m)\left(\frac{1}{2} - \frac{z}{2h}\right)^n \quad (1)$$

$$\rho(z) = \rho_m + (\rho_c - \rho_m)\left(\frac{1}{2} - \frac{z}{2h}\right)^n \quad (2)$$

in which E and ρ are the modulus of elasticity and density, respectively. Subscripts c and m express ceramic and metal materials, respectively, and n represents the power-law index. The displacement field is defined as follows using the assumptions of the four-variable refined plate theory (Thai and Choi 2013a):

$$u(x,y,z) = u_0(x,y) - z\frac{\partial w_b(x,y)}{\partial x} - f(z)\frac{\partial w_s(x,y)}{\partial x} \quad (3)$$

$$v(x,y,z) = v_0(x,y) - z\frac{\partial w_b(x,y)}{\partial y} - f(z)\frac{\partial w_s(x,y)}{\partial y} \quad (4)$$

$$w(x,y,z) = w_b(x,y) + w_s(x,y) \quad (5)$$

where $u_0$and v_0 stand for the in-plane displacements in the x and y directions of the middle plane, w_b and w_s are the bending and shear components of transverse displacement.

The strain-displacement relationships are as follows:

$$\begin{Bmatrix}\varepsilon_x\\ \varepsilon_y\\ \gamma_{xy}\end{Bmatrix} = \begin{Bmatrix}\frac{\partial u_0}{\partial x}\\ \frac{\partial v_0}{\partial y}\\ \frac{\partial u_0}{\partial y}+\frac{\partial v_0}{\partial x}\end{Bmatrix} - z\begin{Bmatrix}\frac{\partial^2 w_b}{\partial x^2}\\ \frac{\partial^2 w_b}{\partial y^2}\\ 2\frac{\partial^2 w_b}{\partial x\partial y}\end{Bmatrix} - f(z)\begin{Bmatrix}\frac{\partial^2 w_s}{\partial x^2}\\ \frac{\partial^2 w_s}{\partial y^2}\\ 2\frac{\partial^2 w_s}{\partial x\partial y}\end{Bmatrix} \quad (6)$$

$$\begin{Bmatrix}\gamma_{yz}\\ \gamma_{xz}\end{Bmatrix} = g(z)\begin{Bmatrix}\frac{\partial w_s}{\partial y}\\ \frac{\partial w_s}{\partial x}\end{Bmatrix}, \qquad \varepsilon_z = 0 \quad (7)$$

where:

$$f(z) = -\frac{z}{4} + \frac{5z^3}{3(2h+2h_p)^2} \quad (8)$$

$$g(z) = 1 - \frac{df(z)}{dz} = \frac{5}{4} - 5\left(\frac{z}{2h+2h_p}\right)^2 \quad (9)$$

The coupled constitutive equations for the piezoelectric layer are expressed as (Tiersten 2013):

$$\begin{aligned}\sigma &= C\varepsilon - e\Xi\\ D &= e^T\varepsilon + \eta\Xi\end{aligned} \quad (10)$$

in which C represents the stress-reduced stiffness matrix, D and Ξ are vectors demonstrating electrical displacement and electric field intensity, respectively, η is the dielectric constant matrix, e represents the piezoelectric constants matrix, σ and ε are stress and strain tensors, respectively. For a transversely isotropic piezoelectric layer, Eq. (11) holds.

$$\begin{Bmatrix}\sigma_{xx}\\ \sigma_{yy}\\ \sigma_{xy}\\ \sigma_{xz}\\ \sigma_{yz}\end{Bmatrix} = \begin{bmatrix}\bar{C}_{11} & \bar{C}_{12} & 0 & 0 & 0\\ \bar{C}_{12} & \bar{C}_{11} & 0 & 0 & 0\\ 0 & 0 & \frac{1}{2}(\bar{C}_{11}-\bar{C}_{12}) & 0 & 0\\ 0 & 0 & 0 & C_{55} & 0\\ 0 & 0 & 0 & 0 & C_{55}\end{bmatrix}\begin{Bmatrix}\varepsilon_{xx}\\ \varepsilon_{yy}\\ \gamma_{xy}\\ \gamma_{xz}\\ \gamma_{yz}\end{Bmatrix} - \begin{bmatrix}0 & 0 & \bar{e}_{31}\\ 0 & 0 & \bar{e}_{31}\\ 0 & 0 & 0\\ -e_{51} & 0 & 0\\ 0 & -e_{51} & 0\end{bmatrix}\begin{bmatrix}\Xi_x\\ \Xi_y\\ \Xi_z\end{bmatrix}$$

$$\begin{bmatrix}D_x\\ D_y\\ D_z\end{bmatrix} = \begin{bmatrix}0 & 0 & 0 & e_{51} & 0\\ 0 & 0 & 0 & 0 & e_{51}\\ \bar{e}_{31} & \bar{e}_{31} & 0 & 0 & 0\end{bmatrix}\begin{Bmatrix}\varepsilon_{xx}\\ \varepsilon_{yy}\\ \gamma_{xy}\\ \gamma_{xz}\\ \gamma_{yz}\end{Bmatrix} + \begin{bmatrix}\eta_{11} & 0 & 0\\ 0 & \eta_{11} & 0\\ 0 & 0 & \bar{\eta}_{33}\end{bmatrix}\begin{bmatrix}\Xi_x\\ \Xi_y\\ \Xi_z\end{bmatrix} \quad (11)$$

$$\phi(x,y,z) = \begin{cases}\varphi(x,y)\left[1-\left(\frac{z-h-\frac{h_p}{2}}{h_p/2}\right)^2\right], & h \le z \le h+h_p\\ \varphi(x,y)\left[1-\left(\frac{-z-h-\frac{h_p}{2}}{h_p/2}\right)^2\right], & -h-h_p \le z \le -h\end{cases} \quad (12)$$

Assuming that each piezoelectric layer is closed-circuit, a quadratic function can be considered for the variation of ϕ through the plate thickness (Wang *et al.* 2001). The electric field Ξ and electric potential ϕ are thought to have a connection that is:

$$\Xi = -\nabla\phi \quad (13)$$

Additionally, the FG core plate's constitutive equations are given as follows:

$$\begin{Bmatrix}\sigma_{xx}\\ \sigma_{yy}\\ \sigma_{xy}\\ \sigma_{xz}\\ \sigma_{yz}\end{Bmatrix} = \begin{bmatrix}Q_{11} & Q_{12} & 0 & 0 & 0\\ Q_{12} & Q_{11} & 0 & 0 & 0\\ 0 & 0 & Q_{66} & 0 & 0\\ 0 & 0 & 0 & Q_{66} & 0\\ 0 & 0 & 0 & 0 & Q_{66}\end{bmatrix}\begin{Bmatrix}\varepsilon_{xx}\\ \varepsilon_{yy}\\ \gamma_{xy}\\ \gamma_{xz}\\ \gamma_{yz}\end{Bmatrix} \quad (14)$$

The matrix components in Eqs. (11) and (14) are given in Appendix A.

2.2 Governing equations

The governing equations can be extracted using the virtual work principle.

$$\delta(U-W)=0 \tag{15}$$

in which U is the strain energy and W is the work done by external work defined as:

$$U=\int_V \sigma_{ij}\varepsilon_{ij}dV=\int_V(\sigma_x\varepsilon_x+\sigma_y\varepsilon_y+\sigma_{xy}\gamma_{xy}+\sigma_{yz}\gamma_{yz}+\sigma_{xz}\gamma_{xz})dV \tag{16}$$

$$W=\int_\Omega qwd\Omega \tag{17}$$

where V is the plate volume and Ω is the surface on which the external load is applied. Substituting the Eqs. (16)-(17) into (15) yields:

$$\begin{aligned}\delta U-\delta W=\int_\Omega\Big(&N_x\delta\Big(\frac{\partial u_0}{\partial x}\Big)+N_y\delta\Big(\frac{\partial v_0}{\partial y}\Big)+N_{xy}\delta\Big(\frac{\partial u_0}{\partial y}+\frac{\partial v_0}{\partial x}\Big)-M_x^b\delta\Big(\frac{\partial^2 w_b}{\partial x^2}\Big)\\&-M_y^b\delta\Big(\frac{\partial^2 w_b}{\partial y^2}\Big)-M_x^s\delta\Big(\frac{\partial^2 w_s}{\partial x^2}\Big)-2M_{xy}^b\delta\Big(\frac{\partial^2 w_b}{\partial x\partial y}\Big)-M_y^s\delta\Big(\frac{\partial^2 w_s}{\partial y^2}\Big)\\&-2M_{xy}^s\delta\Big(\frac{\partial^2 w_s}{\partial x\partial y}\Big)+S_{yz}\delta\Big(\frac{\partial w_s}{\partial y}\Big)+S_{xz}\delta\Big(\frac{\partial w_s}{\partial x}\Big)\Big)d\Omega\\&-\int_\Omega q(\delta w_b+\delta w_s)d\Omega=0\end{aligned} \tag{18}$$

in which the stress resultants are defined as:

$$\begin{Bmatrix}N_i\\M_i^b\\M_i^s\end{Bmatrix}=\int_{-h-h_p}^{h+h_p}\sigma_i\begin{Bmatrix}1\\z\\f\end{Bmatrix}dz\ ,\ (i=x,y,xy)$$

$$S_i=\int_{-h-h_p}^{h+h_p}g\sigma_i\ dz\ ,\ (i=xz,yz) \tag{19}$$

Performing the integration by parts and collecting the factors of δu_0, δv_0, δw_b and δw_s lead to four governing equations:

$$\delta u_0:\quad \frac{\partial N_x}{\partial x}+\frac{\partial N_{xy}}{\partial y}=0 \tag{20a}$$

$$\delta v_0:\quad \frac{\partial N_y}{\partial y}+\frac{\partial N_{xy}}{\partial x}=0 \tag{20b}$$

$$\delta w_b:\quad \frac{\partial^2 M_x^b}{\partial x^2}+\frac{\partial^2 M_y^b}{\partial y^2}+2\frac{\partial^2 M_{xy}^b}{\partial x\partial y}+q=0 \tag{20c}$$

$$\delta w_s:\quad \frac{\partial^2 M_x^s}{\partial x^2}+\frac{\partial^2 M_y^s}{\partial y^2}+2\frac{\partial^2 M_{xy}^s}{\partial x\partial y}+\frac{\partial S_{yz}}{\partial y}+\frac{\partial S_{xz}}{\partial x}+q=0 \tag{20d}$$

Substituting Eqs. (6)-(7) and Eq. (10) into Eq. (19) yields:

$$\begin{Bmatrix}N\\M^b\\M^s\end{Bmatrix}=\begin{bmatrix}A&B&B^s\\B&D&D^s\\B^s&D^s&H\end{bmatrix}\begin{Bmatrix}\varepsilon\\\kappa^b\\\kappa^s\end{Bmatrix}-\begin{bmatrix}0&K&T\end{bmatrix}\varphi$$

$$S=A^s\gamma+\mu_3\Gamma \tag{21}$$

Eq. (21) components are noted in Appendix A. By putting Eq. (21) into Eqs. (20), governing equations of the plate can be rewritten as given in Eqs. (22):

$$\begin{aligned}&A_{11}\frac{\partial^2 u_0}{\partial x^2}+A_{66}\frac{\partial^2 u_0}{\partial y^2}+(A_{12}+A_{66})\frac{\partial^2 v_0}{\partial x\partial y}\\&-B_{11}\frac{\partial^3 w_b}{\partial x^3}-(B_{12}+2B_{66})\frac{\partial^3 w_b}{\partial x\partial y^2}\\&-B_{11}^s\frac{\partial^3 w_s}{\partial x^3}-(B_{12}^s+2B_{66}^s)\frac{\partial^3 W_s}{\partial x\partial y^2}=0\end{aligned} \tag{22a}$$

$$\begin{aligned}&A_{22}\frac{\partial^2 v_0}{\partial y^2}+A_{66}\frac{\partial^2 v_0}{\partial x^2}+(A_{12}+A_{66})\frac{\partial^2 u_0}{\partial x\partial y}\\&-B_{22}\frac{\partial^3 w_b}{\partial y^3}-(B_{12}+2B_{66})\frac{\partial^3 w_b}{\partial x^2\partial y}\\&-B_{22}^s\frac{\partial^3 w_s}{\partial y^3}-(B_{12}^s+2B_{66}^s)\frac{\partial^3 w_s}{\partial x^2\partial y}=0\end{aligned} \tag{22b}$$

$$\begin{aligned}&B_{11}\frac{\partial^3 u_0}{\partial x^3}+(B_{12}+2B_{66})\frac{\partial^3 u_0}{\partial x\partial y^2}+B_{22}\frac{\partial^3 v_0}{\partial y^3}\\&+(B_{12}+2B_{66})\frac{\partial^3 v_0}{\partial x^2\partial y}-D_{11}\frac{\partial^4 w_b}{\partial x^4}\\&-(2D_{12}+4D_{66})\frac{\partial^4 w_b}{\partial x^2\partial y^2}-D_{22}\frac{\partial^4 w_b}{\partial y^4}\\&-D_{11}^s\frac{\partial^4 w_s}{\partial x^4}-(2D_{12}^s+4D_{66}^s)\frac{\partial^4 w_s}{\partial x^2\partial y^2}\\&-D_{22}^s\frac{\partial^4 w_s}{\partial y^4}-\mu_1\Big(\frac{\partial^2\varphi}{\partial x^2}+\frac{\partial^2\varphi}{\partial y^2}\Big)+q=0\end{aligned} \tag{22c}$$

$$\begin{aligned}&B_{11}^s\frac{\partial^3 u_0}{\partial x^3}+B_{22}^s\frac{\partial^3 v_0}{\partial y^3}+(B_{12}^s+2B_{66}^s)\frac{\partial^3 u_0}{\partial x\partial y^2}\\&+(B_{12}^s+2B_{66}^s)\frac{\partial^3 v_0}{\partial x^2\partial y}-D_{11}^s\frac{\partial^4 w_b}{\partial x^4}\\&-(2D_{12}^s+4D_{66}^s)\frac{\partial^4 w_b}{\partial x^2\partial y^2}-D_{22}^s\frac{\partial^4 w_b}{\partial y^4}\\&-H_{11}\frac{\partial^4 w_s}{\partial x^4}-(2H_{12}+4H_{66})\frac{\partial^4 w_s}{\partial x^2\partial y^2}\\&-H_{22}\frac{\partial^4 w_s}{\partial y^4}+A_{11}^s\Big(\frac{\partial^2 w_s}{\partial x^2}+\frac{\partial^2 w_s}{\partial y^2}\Big)\\&+(\mu_3-\mu_2)\Big(\frac{\partial^2\varphi}{\partial x^2}+\frac{\partial^2\varphi}{\partial y^2}\Big)+q=0\end{aligned} \tag{22d}$$

where **A** indicates in-plane stiffness, $\mathbf{A}^{s}$ describes in-plane shear stiffness, **B** represents the coupling between in-plane forces and bending moments, and $\mathbf{B}^{s}$ denotes shear coupling. **D** represents bending stiffness, $\mathbf{D}^{s}$ illustrates shear bending stiffness, and **H** represents higher-order stiffnesses and coupling. The parameters μ_i represent the interaction effects between piezoelectric influences and mechanical responses. These parameters are determined by integrating material properties across the plate's thickness and are detailed in Appendix A.

Maxwell's equation should be satisfied in piezoelectric layers by the following relation:

$$\int_{h}^{h+h_p} \vec{\nabla} . \vec{\boldsymbol{d}} dz + \int_{-h-h_p}^{-h} \vec{\nabla} . \vec{\boldsymbol{d}} dz = 0 \quad (23)$$

Substituting the second Eq. of (10) into (23) yields:

$$\Upsilon_1 \nabla^2 w_s - \Upsilon_2 \nabla^2 \varphi - \Upsilon_3 \nabla^2 w_b + \Upsilon_4 \varphi = 0 \quad (24)$$

where the Υ_i coefficients describe the interaction between mechanical and electrical fields in piezoelectric materials and are provided in Appendix A. Eqs. (22) and Eq. (24) are five differential equations with five unknown variables (u_0, v_0, w_b, w_s, and φ).

In the subsequent examples presented in Section 3, various materials are employed. Table 1 summarizes the properties of the materials used in these numerical examples.

Table 1 Material properties (Abad and Rouzegar 2017).

Property	Core plate			Piezoelectric layer
	Al	Al_2O_3		PZT-4
E(GPa)	70	380		-
υ	0.3	0.3		-
C_{11}(GPa)	-	-		132
C_{12}(GPa)	-	-		71
C_{33}(GPa)	-	-		115
C_{13}(GPa)	-	-		73
C_{55}(GPa)	-	-		26
e_{31}(cm^{-2})	-	-		-4.1
e_{33}(cm^{-2})	-	-		14.1
e_{15}(cm^{-2})	-	-		10.5
η_{11}(nFm^{-1})	-	-		7.124
η_{33}(nFm^{-1})	-	-		5.841
ρ(kgm^{-3})	2707	3800		7500

2.3 Levy's solution and State-Space approach

The plate is electrically insulated at four edges and has simply supported boundary conditions at x=0 and x=a, which results in the following:

$$v_0 = w_b = w_s = N_x = M_x^b = M_x^s = \varphi = 0 \quad (25)$$

while edges y=b/2 and y=-b/2 may be arbitrarily chosen as simply supported, clamped or free (introduced in Appendix B). Considering Levy's solution procedure, the components of displacement and electrostatic potential satisfying simply supported conditions at x=0 and x=a are expressed as follows:

$$\begin{Bmatrix} u_0(x,y) \\ v_0(x,y) \\ w_b(x,y) \\ w_s(x,y) \\ \varphi(x,y) \end{Bmatrix} = \sum_{m=1}^{\infty} \begin{Bmatrix} U_m(y)\ cos(\alpha x) \\ V_m(y)\ sin(\alpha x) \\ W_{bm}(y)\ sin(\alpha x) \\ W_{sm}(y)\ sin(\alpha x) \\ \varphi_m(y)\ sin(\alpha x) \end{Bmatrix} \quad (26)$$

where $\alpha = \frac{m\pi}{a}$ and $U_m(y)$, $V_m(y)$, $W_{bm}(y)$, $W_{sm}(y)$ and $\varphi_m(y)$ are unknown functions. The single form of the Fourier series is used to extend the transverse external load applied on the plate as follows:

$$q(x,y) = \sum_{m=1}^{\infty} Q_m(y)\ sin(\alpha x) \quad (27)$$

$$Q_m(y) = \frac{2}{a}\int_0^a q(x,y)\ sin(\alpha x) dx \quad (28)$$

in which the coefficient $Q_m(y)$ is determined as follows for the case of uniformly distributed load q_0:

$$Q_m(y) = \frac{4q_0}{m\pi} \quad (29)$$

Substituting Eq. (26) into Eqs. (22) and Eq. (24) results in an ordinary differential system of equations:

$$U_m'' = c_1 U_m + c_2 V_m' + c_3 W_{bm} + c_4 W_{bm}'' + c_{3s} W_{sm} + c_{4s} W_{sm}'' \quad (30a)$$

$$V_m'' = c_5 U_m' + c_6 V_m + c_7 W_{bm}' + c_8 W_{bm}''' + c_{7s} W_{sm}' + c_{8s} W_{sm}''' \quad (30b)$$

$$W_{bm}'''' = c_9 U_m + c_{10} V_m' + c_{11} W_{bm} + c_{12} W_{bm}'' + c_{13} W_{sm} + c_{14} W_{sm}'' + c_{16} \varphi_m + c_{15} Q_m \quad (30c)$$

$$W_{sm}'''' = c_{9s} U_m + c_{10s} V_m' + c_{11s} W_{bm} + c_{12s} W_{bm}'' + c_{13s} W_{sm} + c_{14s} W_{sm}'' + c_{16s} \varphi_m + c_{15s} Q_m \quad (30d)$$

$$\varphi_m'' = c_{11m} W_{bm} + c_{12m} W_{bm}'' + c_{13m} W_{sm} + c_{14m} W_{sm}'' + c_{16m} \varphi_m \quad (30e)$$

where $()' = \frac{d}{dy}$ and coefficients c_{ij} are given in Appendix B. Also, the boundary conditions at y=b/2 and y=-b/2 are written in terms of ($U_m(y)$, $V_m(y)$, $W_{bm}(y)$, $W_{sm}(y)$ and $\varphi_m(y)$) and given in Appendix B. The state-space concept deals with coupled fourth-order differential equations defined by Eqs. (30), which can be rewritten as follows:

$$\mathbf{X}'(y) = \mathbf{G}\mathbf{X}(y) + \mathbf{F} \quad (31)$$

in which $\mathbf{X}(y)$, **G** and **F** are the state vector, transfer matrix and force vector, respectively, which are defined as:

$$\{\mathbf{X}(y)\} = \{U_m \quad U_m' \quad V_m \quad V_m' \quad \varphi_m \quad \varphi_m' \quad W_{bm} \quad W_{bm}' \quad W_{bm}'' \quad W_{bm}''' \quad W_{sm} \quad W_{sm}' \quad W_{sm}'' \quad W_{sm}'''\}^T \quad (32)$$

$$\{\mathbf{F}\} = \{0 \quad 0 \quad 0 \quad 0 \quad 0 \quad 0 \quad 0 \quad 0 \quad 0 \quad c_{15}Q_m \quad 0 \quad 0 \quad 0 \quad c_{15s}Q_m\}^T \tag{33}$$

$$\mathbf{G} = \begin{bmatrix}
0 & 1 & 0 & 0 & 0 & 0 & 0 & 0 & 0 & 0 & 0 & 0 & 0 & 0 \\
c_1 & 0 & 0 & c_2 & 0 & 0 & c_3 & 0 & c_4 & 0 & c_{3s} & 0 & c_{4s} & 0 \\
0 & 0 & 0 & 1 & 0 & 0 & 0 & 0 & 0 & 0 & 0 & 0 & 0 & 0 \\
0 & c_5 & c_6 & 0 & 0 & 0 & 0 & c_7 & 0 & c_8 & 0 & c_{7s} & 0 & c_{8s} \\
0 & 0 & 0 & 0 & 0 & 1 & 0 & 0 & 0 & 0 & 0 & 0 & 0 & 0 \\
0 & 0 & 0 & 0 & c_{16m} & 0 & c_{11m} & 0 & c_{12m} & 0 & c_{13m} & 0 & c_{14m} & 0 \\
0 & 0 & 0 & 0 & 0 & 0 & 0 & 1 & 0 & 0 & 0 & 0 & 0 & 0 \\
0 & 0 & 0 & 0 & 0 & 0 & 0 & 0 & 1 & 0 & 0 & 0 & 0 & 0 \\
0 & 0 & 0 & 0 & 0 & 0 & 0 & 0 & 0 & 1 & 0 & 0 & 0 & 0 \\
c_9 & 0 & 0 & c_{10} & c_{16} & 0 & c_{11} & 0 & c_{12} & 0 & c_{13} & 0 & c_{14} & 0 \\
0 & 0 & 0 & 0 & 0 & 0 & 0 & 0 & 0 & 0 & 0 & 1 & 0 & 0 \\
0 & 0 & 0 & 0 & 0 & 0 & 0 & 0 & 0 & 0 & 0 & 0 & 1 & 0 \\
0 & 0 & 0 & 0 & 0 & 0 & 0 & 0 & 0 & 0 & 0 & 0 & 0 & 1 \\
c_{9s} & 0 & 0 & c_{10s} & c_{16s} & 0 & c_{11s} & 0 & c_{12s} & 0 & c_{13s} & 0 & c_{14s} & 0
\end{bmatrix} \tag{34}$$

The solution for the state-space Eq. (31) can be expressed as (Franklin 2012):

$$\mathbf{X}(y) = e^{\mathbf{G}y}\mathbf{k} + e^{\mathbf{G}y}\int_0^y e^{-\mathbf{G}\zeta}\,\mathbf{F}d\zeta \tag{35}$$

where $\mathbf{k}$ is a constant vector identified by applying conditions of y=b/2 and y=-b/2. $e^{\mathbf{G}y}$ is determined as:

$$e^{\mathbf{G}y} = \mathbf{R}\begin{bmatrix} e^{\lambda_1 y} & \cdots & 0 \\ \vdots & \ddots & \vdots \\ 0 & \cdots & e^{\lambda_{14} y} \end{bmatrix}\mathbf{R}^{-1} \tag{36}$$

where λ_i and $\mathbf{R}$ stand for the distinct eigenvalues and the eigenvector of $\mathbf{G}$, respectively. To avoid the problems of ill-conditioning, Eq. (35) is rewritten as below:

$$\mathbf{X}(y) = \mathbf{R}\begin{bmatrix} e^{\lambda_1 y} & \cdots & 0 \\ \vdots & \ddots & \vdots \\ 0 & \cdots & e^{\lambda_{14} y} \end{bmatrix}\mathbf{P} + e^{\mathbf{G}y}\int_0^y e^{-\mathbf{G}\zeta}\,\mathbf{F}d\zeta \tag{37}$$

where

$$\mathbf{P} = \mathbf{R}^{-1}\mathbf{k} \tag{38}$$

Boundary conditions at y=b/2 and y=-b/2 should be expressed in terms of the state vector to determine the constant vector $\mathbf{P}$.

3. Results and discussion

Several examples are solved to demonstrate the accuracy and effectiveness of the suggested approach for forecasting the bending behavior of rectangular plate constructions. The upper surface of the structure is subjected to a uniformly distributed load in the transverse direction. For simplicity, the plate boundary condition is expressed as SXSY, in which S stands for simply supported conditions at x=0 and x=a. The arbitrary circumstances at y=b/2 and y=-b/2 are denoted simultaneously by X and Y, respectively.

The number of required terms in Levy's series solution to achieve converged results is different for various cases and boundary conditions. In this research, the convergence criterion is considered as: $(\left|(X_{m+1} - X_m)/X_{m+1}\right| < 10^{-4})$. The convergence of deflection and stresses are checked, so $\boldsymbol{X_m}$ and $\boldsymbol{X_{m+1}}$ in the above relation ate two consecutive deflections or stresses. According to the above-mentioned criterion, the number of terms necessary to achieve converged results are 23, 27, 25, 23, 21, and 19 terms for the SSSS, SCSC, SSSC, SFSC, SSSF, and SFSF smart FG plates, respectively; and are 25, 27, 25, 23, 21 and 19 terms for the SSSS, SCSC, SSSC, SFSC, SSSF, and SFSF smart transversely isotropic plate, respectively. The number of terms required for convergence and the corresponding computational costs are illustrated in a bar chart in Fig. 2 for different boundary conditions. This research and its findings were conducted using a system with an Intel(R) Core (TM) i7-1065G7 CPU @ 1.30GHz.

Since no significant results exist for the bending analysis of plates sandwiched between two closed-circuit piezoelectric layers exposed to uniformly distributed loads, the commercial Abaqus package is used to validate the bending results. For this purpose, different layers of the hybrid structure are initially modelled and assembled, and proper material properties are defined. Following this, the tie contact is considered between layers (it is assumed that piezoelectric layers are fully bonded to the base plate). Afterwards, loadings and boundary conditions are implied on the surfaces and edges of the structure. Since the Abaqus package does not include a shell element for the piezoelectric layer, the whole structure is modeled by solid elements. C3D8E and C3D8R elements are employed to discretize the piezoelectric layers and the base plate, respectively. A convergence study is performed to ensure the independence of the results from the mesh structure. The number of elements via the thickness of the core plate and each piezoelectric layer for the smart transversely isotropic plate is 8 and 1, respectively, and a total of 400000 elements are taken into account for the mesh structure. For the smart FG plate analysis, the number of elements through the thickness of the core plate is 16, while it is 2 for each piezoelectric layer, and 120 elements are considered along the plate length and width. Unless otherwise mentioned, non-dimensional parameters are expressed as given in Eq. (39):

Example 1. In the first example, the bending behavior of a square FG plate made of Al/Al_2O_3 with different power- law

$$\overline{W} = \frac{10h^3E_c}{q_0a^4}w(\frac{a}{2},0,0), \qquad \bar{\varepsilon}_x = \varepsilon_x(\frac{a}{2},0,\frac{h}{2}),$$
$$\bar{\sigma}_x = \frac{h}{q_0a}\sigma_x(\frac{a}{2},0,\frac{h}{2}), \qquad \bar{\tau}_{xz} = \frac{h}{q_0a}\tau_{xz}(\frac{a}{4},\frac{b}{4},-\frac{h}{4}) \tag{39}$$

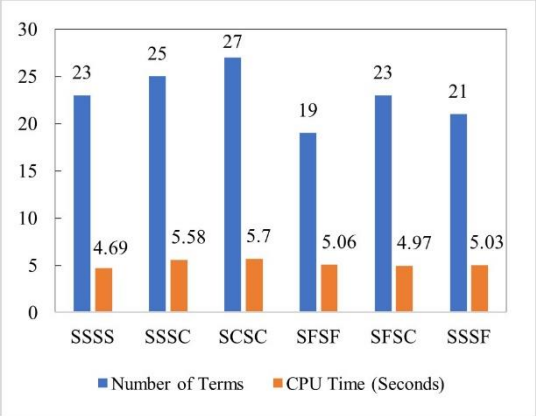

(a)

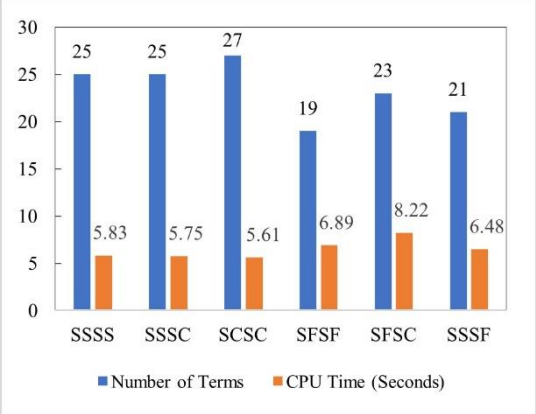

(b)

Fig. 2 Number of terms for convergence and computational cost for: a) smart FG plate; b) smart transversely isotr opic plate.

indices subjected to uniformly distributed load q_0 is investigated. The non-dimensional parameters are expressed as:

$$\overline{W} = \frac{10h^3E_c}{q_0a^4}w\left(\frac{a}{2},\frac{b}{2},0\right), \quad \bar{\sigma}_x = \frac{h}{q_0a}\sigma_x\left(\frac{a}{2},\frac{b}{2},\frac{h}{3}\right)$$
$$\bar{\sigma}_{xy} = \frac{h}{q_0a}\sigma_{xy}\left(0,0,-\frac{h}{3}\right), \bar{\sigma}_{xz} = \frac{h}{q_0a}\sigma_{xz}\left(0,\frac{b}{2},\frac{h}{6}\right) \tag{40}$$
$$\bar{\sigma}_{yz} = \frac{h}{q_0a}\sigma_{yz}(\frac{a}{2},0,0)$$

Table 2 compares the non-dimensional values of stresses and deflection of a fully simply supported plate with a/h=10 obtained by the current method and the results reported by SSDT (Zenkour 2006) and HSDT (Thai and Choi 2013b). The present results based on the four-variable RPT match well with other methods, particularly with the HSDT results, which prove the precision and accuracy of the proposed approach. It should be mentioned that the utilized plate theory, with only four unknown variables, is less complex than the HSDT.

Table 2 Non-dimensional deflection and stresses of a square FG plate with SSSS boundary conditions (a/h=10).

n	Theory	$\bar{W}$	$\bar{\sigma}_x$	$\bar{\sigma}_{xy}$	$\bar{\sigma}_{xz}$	$\bar{\sigma}_{yz}$
0	Present	0.4666	1.9106	1.2848	0.4424	0.4977
	SSDT[1]	0.4665	1.9103	1.2850	0.4429	0.5114
	HSDT[2]	0.4666	1.9106	1.2856	0.4409	0.4949
1	Present	0.9288	2.1697	1.1141	0.5440	0.4977
	SSDT	0.9287	2.1692	1.1143	0.5446	0.5114
	HSDT	0.9288	2.1696	1.1146	0.5422	0.4949
2	Present	1.1940	2.0345	0.9907	0.5702	0.4554
	SSDT	1.1940	2.0338	0.9907	0.5734	0.4700
	HSDT	1.1940	2.0345	0.9912	0.5682	0.4528
8	Present	1.5337	1.3841	1.0630	0.4340	0.4235
	SSDT	1.5343	1.3829	1.0628	0.4392	0.4399
	HSDT	1.5336	1.3841	1.0637b	0.4324	0.4210
10	Present	1.5872	1.2831	1.0696	0.4188	0.4394
	SSDT	1.5876	1.2820	1.0694	0.4227	0.4552
	HSDT	1.5872	1.2830	1.0703	0.4174	0.4369

[1] (Zenkour 2006); [2] (Thai and Choi 2013b)

The non-dimensional central deflection of the FG square plate with different boundary conditions is listed in Table 3. A comparison between the FE results reported by Thai and Choi (2013c) and those obtained by the proposed approach verifies the accuracy of the current procedure. As expected, the plate deflection increases by decreasing the constraints from SCSC to SFSF boundary condition. Additionally, as the power-law index rises and the plate transitions from pure ceramic (Al_2O_3) to pure metal (Al), the deflection rises because of the elastic modulus and accordingly, the stiffness of the Al_2O_3 plate is higher than that of Al.

Example 2. A hybrid rectangular plate with a transversely isotropic core having two PZT-4 layers at the upper and lower surfaces is considered. The core plate is made of Al_2O_3 with the following properties (Abad and Rouzegar 2019):

$$C_{11} = 460.2 \text{ GPa}, \quad C_{12} = 174.7 \text{ GPa},$$
$$C_{33} = 509.5 \text{ GPa}, \quad C_{13} = 127.4 \text{ GPa},$$
$$C_{55} = 126.9 \ GPa, \quad \rho = 4000 \ kg/m^3 \tag{41}$$

The non-dimensional deflection in this example is defined as below:

$$\overline{W} = \frac{10h^3\bar{C}_{11}}{q_0a^4}w(\frac{a}{2},0,0) \tag{42}$$

Since there is no existing result in the literature for the prescribed problem, the obtained results by the proposed approach are compared with the FE simulation using the Abaqus package. Table 4 demonstrates the obtained results for the smart plate with $h_p/2h$=0.1 having various boundary conditions and thickness-to-side ratios. The satisfactory agreement between the results shows that the proposed Levy's solution and the state-space approach are accurate and effective. Also, As can be seen, the non-dimensional deflection increases by increasing the thickness-to-side ratio,

which is related to the definition $\overline{W}$ in Eq. (42).

Table 3 Non-dimensional central deflection of the square FG plate with different boundary conditions.

a/h	*n*	Method	Boundary conditions					
			SCSC	SSSC	SSSS	SFSC	SFSS	SFSF
5	0	Present	0.2990	0.3949	0.5354	0.7386	0.9871	1.5857
		FEM[1]	0.3090	0.4020	0.5381	0.7579	0.9986	1.6153
	0.5	Present	0.4443	0.5920	0.8085	1.1168	1.4997	2.4165
		FEM	0.4577	0.6015	0.8120	1.1431	1.5153	2.4570
	5	Present	0.9711	1.2642	1.6929	2.3299	3.0871	4.9318
		FEM	0.9896	1.2770	1.6973	2.3685	3.1091	4.9908
	10	Present	1.1121	1.4346	1.9060	2.6195	3.4517	5.4949
		FEM	1.1365	1.4518	1.9125	2.6697	3.4814	5.5730
10	0	Present	0.2321	0.3270	0.4666	0.6490	0.8963	1.4688
		FEM	0.2424	0.3343	0.4693	0.6684	0.9079	1.4985
	0.5	Present	0.3537	0.5001	0.7154	0.9954	1.3770	2.2584
		FEM	0.3676	0.5099	0.7190	1.0221	1.3925	2.2990
	5	Present	0.7215	1.0104	1.4349	1.9945	2.7467	4.4934
		FEM	0.7406	1.0235	1.4393	2.0335	2.7687	4.5524
	10	Present	0.8038	1.1211	1.5872	2.2052	3.0312	4.9533
		FEM	0.8297	1.1391	1.5937	2.2564	3.0609	5.0316
20	0	Present	0.2151	0.3099	0.4493	0.6264	0.8736	1.4396
		FEM	0.2256	0.3173	0.4521	0.646	0.8851	1.4692
	0.5	Present	0.3307	0.4770	0.6921	0.9649	1.3462	2.2189
		FEM	0.3449	0.4869	0.6956	0.9917	1.3618	2.2594
	5	Present	0.6579	0.9463	1.3703	1.9098	2.6615	4.3837
		FEM	0.6776	0.9597	1.3747	1.9493	2.6835	4.4427
	10	Present	0.7252	1.0418	1.5073	2.1006	2.9259	4.8177
		FEM	0.7521	1.0604	1.5138	2.1525	2.9557	4.8958

[1] (Thai and Choi 2013c)

Fig. 3 illustrates the non-dimensional normal stress ($\bar{\sigma}_x$) across the plate thickness, considering different values of thickness-to-side ratios. The plot indicates that the maximum stress occurs at the interface between the core and piezoelectric layers, while it remains zero at the centre of the core plate, as anticipated. Notably, a sudden change in stress is evident at the interfaces, which can be attributed to the different material properties of the core plate and piezoelectric layers. Also, the data demonstrates that the non-dimensional normal stress gradually decreases as the thickness-to-side ratio increases. This can be explained by the fact that thicker plates experience lower stress compared to thinner plates. The results of this analysis can be valuable in optimizing the design of similar structures to minimize stress concentrations and enhance their performance.

Fig. 4 represents the effect of piezoelectric layer thickness ($h_p/2h$) on the variations of non-dimensional transverse shear stress ($\bar{\tau}_{xz}$) across the thickness of the smart transversely isotropic plate. The transverse shear stress follows a parabolic distribution through the plate thickness,

Table 4 Non-dimensional deflection and normal stress of a transversely isotropic plate with piezoelectric layers ($h_p/2h$ =0.1).

B.Cs.	$2h/a$	Method	$\bar{W}$	$\bar{\sigma}_x$
SSSF	0.05	Present	0.1055	2.1080
			[0.66] *	[0.50]
		Abaqus	0.1062	2.1187
	0.1	Present	0.1090	1.0506
			[0.37]	[0.43]
		Abaqus	0.1094	1.0551
SSSS	0.05	Present	0.0540	1.2843
			[0.37]	[0.53]
		Abaqus	0.0542	1.2911
	0.1	Present	0.0567	0.6394
			[0.35]	[0.47]
		Abaqus	0.0565	0.6424
SCSC	0.05	Present	0.0260	0.6617
			[1.51]	[2.37]
		Abaqus	0.0264	0.6778
	0.1	Present	0.0290	0.3381
			[2.68]	[4.52]
		Abaqus	0.0298	0.3541
SFSF	0.05	Present	0.1738	3.2019
			[0.63]	[0.42]
		Abaqus	0.1749	3.2155
	0.1	Present	0.1782	1.5968
			[0.33]	[0.26]
		Abaqus	0.1788	1.6009
SFSC	0.05	Present	0.0758	1.4864
			[1.30]	[1.43]
		Abaqus	0.0768	1.5079
	0.1	Present	0.0792	0.6199
			[2.58]	[3.98]
		Abaqus	0.0813	0.6456
SSSC	0.05	Present	0.0373	0.9134
			[1.06]	[1.50]
		Abaqus	0.0377	0.9273
	0.1	Present	0.0399	0.4589
			[2.20]	[3.06]
		Abaqus	0.0408	0.4734

$$\%Error = \left|\frac{state\ space\ result - Abaqus\ result}{Abaqus\ result}\right| \times 100$$

with its maximum value occurring at the middle plane, following the utilized plate theory. Furthermore, the results demonstrate that increasing the piezoelectric layer thickness leads to a decrease in stress values, indicating that thicker piezoelectric layers can effectively reduce stresses in the structure. Moreover, the study suggests that thicker piezoelectric layers can enhance the electromechanical coupling effect, leading to reduced deflection and stress.

Example 3. We explore a square FG plate (Al/Al_2O_3) with two PZT-4 layers on the upper and lower surfaces. The non-dimensional deflection, normal stress, and normal strain values are listed in Tables 5-6 for two thickness-to-side ratios of $2h/a$=0.05 and $2h/a$=0.1, respectively. To verify the efficiency of the current method, results are compared with those obtained from Abaqus simulations. It is evident that the theory and method employed in this study yield highly accurate results.

Table 5 Non-dimensional deflection, normal stress, and normal strain in a square FG plate with piezoelectric layers ($2h/a$=0.05).

			$h_p/2h = 0.1$			$h_p/2h = 0.2$		
B.Cs.	n	Method	$\bar{W}$	$\bar{\sigma}_x$	$\bar{\varepsilon}_x * 10^{10}$	$\bar{W}$	$\bar{\sigma}_x$	$\bar{\varepsilon}_x * 10^{10}$
SFSC	Al_2O_3	Present	0.0681 [0.00]	1.4674 [0.24]	1.3141 [0.22]	0.0577 [0.87]	1.2412 [0.62]	1.1114 [0.60]
		Abaqus	0.0681	1.4710	1.3170	0.0572	1.2335	1.1047
	0.5	Present	0.0978	1.6011	2.4213	0.0774	1.2517	1.8924
	5	Present	0.1612	0.9814	4.7487	0.1120	0.6545	3.1656
	Al	Present	0.2358 [1.72]	0.9295 [1.26]	4.5169 [1.28]	0.1458 [2.60]	0.5704 [1.91]	2.7714 [2.10]
		Abaqus	0.2318	0.9179	4.4596	0.1421	0.5597	2.7142
SSSF	Al_2O_3	Present	0.0950 [0.52]	2.0820 [0.54]	1.8704 [0.64]	0.0804 [1.25]	1.7611 [1.47]	1.5820 [1.55]
		Abaqus	0.0945	2.0708	1.8585	0.0794	1.7355	1.5578
	0.5	Present	0.1364	2.2716	3.4462	0.1080	1.7760	2.6939
	5	Present	0.2244	1.3929	6.7617	0.1557	0.9291	4.5090
	Al	Present	0.3283 [2.43]	1.3194 [2.45]	6.4327 [2.57]	0.2027 [3.62]	0.8100 [3.60]	3.9488 [3.91]
		Abaqus	0.3205	1.2878	6.2710	0.1956	0.7818	3.8001
SFSF	Al_2O_3	Present	0.1566 [0.57]	3.1957 [0.63]	3.1404 [0.60]	0.1325 [1.37]	2.7034 [1.60]	2.6563 [1.50]
		Abaqus	0.1557	3.1754	3.1216	0.1307	2.6608	2.6170
	0.5	Present	0.2247	3.4867	5.7860	0.1779	2.7263	4.5231
	5	Present	0.3695	2.1383	11.3534	0.2562	1.4265	7.5716
	Al	Present	0.5405 [2.52]	2.0259 [2.70]	10.8032 [2.58]	0.3333 [3.73]	1.2442 [3.97]	6.6334 [3.88]
		Abaqus	0.5272	1.9726	10.5311	0.3213	1.1966	6.3852
SSSC	Al_2O_3	Present	0.0337 [0.29]	0.8829 [0.40]	0.6069 [0.31]	0.0286 [1.06]	0.7469 [0.52]	0.5134 [1.42]
		Abaqus	0.0336	0.8865	0.6050	0.0283	0.7430	0.5062
	0.5	Present	0.0484	0.9635	1.1187	0.0384	0.7533	0.8746
	5	Present	0.0801	0.5906	2.1943	0.0558	0.3938	1.4631
	Al	Present	0.1172 [2.26]	0.5591 [1.02]	2.0864 [2.20]	0.0728 [3.40]	0.3430 [1.57]	1.2796 [3.50]
		Abaqus	0.1146	0.5534	2.0414	0.0704	0.3377	1.2363
SCSC	Al_2O_3	Present	0.0234 [0.00]	0.6350 [1.21]	0.3949 [0.40]	0.0199 [1.01]	0.5371 [0.33]	0.3340 [0.76]
		Abaqus	0.0234	0.6428	0.3965	0.0197	0.5389	0.331473
	0.5	Present	0.0336	0.6931	0.7280	0.0267	0.5418	0.5690
	5	Present	0.0558	0.4246	1.4269	0.0390	0.2830	0.9508
	Al	Present	0.0816 [1.61]	0.4018 [0.19]	1.3558 [1.05]	0.0509 [2.41]	0.2463 [0.16]	0.8306 [2.06]
		Abaqus	0.0803	0.4026	1.3416	0.0497	0.2467	0.8138
SSSS	Al_2O_3	Present	0.0489 [0.82]	1.2483 [0.46]	0.9198 [1.18]	0.0414 [1.71]	1.0560 [1.46]	0.7781 [2.30]
		Abaqus	0.0485	1.2425	0.9090	0.0407	1.0408	0.7606
	0.5	Present	0.0702	1.3622	1.6952	0.0556	1.0651	1.3254
	5	Present	0.1158	0.8352	3.3266	0.0805	0.5571	2.2188
	Al	Present	0.1694 [2.97]	0.7910 [2.34]	3.1641 [3.47]	0.1039 [3.49]	0.4855 [3.44]	1.9301 [4.60]
		Abaqus	0.1645	0.7729	3.0578	0.1004	0.4693	1.8452

*$[\%Error] = \left|\frac{state\ space\ result - Abaqus\ result}{Abaqus\ result}\right| \times 100$

Table 6 Non-dimensional deflection, normal stress, and normal strain of a square smart FG plate ($2h/a$=0.1).

			$h_p/2h = 0.1$			$h_p/2h = 0.2$		
B.Cs.	n	Method	$\bar{W}$	$\bar{\sigma}_x$	$\bar{\varepsilon}_x * 10^{10}$	$\bar{W}$	$\bar{\sigma}_x$	$\bar{\varepsilon}_x * 10^{10}$
SFSC	Al_2O_3	Present	0.0708 [0.97]	0.7308 [2.78]	0.3273 [1.97]	0.0601 [0.33]	0.6180 [1.87]	0.2767 [1.00]
		Abaqus	0.0715	0.7517	0.3339	0.0603	0.6298	0.2795
	0.5	Present	0.1013	0.7981	0.6035	0.0806	0.6233	0.4712
	5	Present	0.1700	0.4878	1.1804	0.1194	0.3244	0.7850
	Al	Present	0.2483 [0.08]	0.4608 [2.94]	1.1201 [1.57]	0.1566 [0.57]	0.2845 [2.90]	0.6843 [1.41]
		Abaqus	0.2481	0.4748	1.1380	0.1557	0.2930	0.6941
SSSF	Al_2O_3	Present	0.0977 [0.82]	1.0381 [0.38]	0.4663 [1.30]	0.0828 [1.71]	0.8780 [1.59]	0.3944 [2.60]
		Abaqus	0.0969	1.0341	0.4603	0.0814	0.8642	0.3844
	0.5	Present	0.1399	1.1333	0.8597	0.1111	0.8854	0.6716
	5	Present	0.2333	0.6935	1.6836	0.1632	0.4617	1.1208
	Al	Present	0.3410 [2.58]	0.6558 [1.56]	1.5990 [3.09]	0.2135 [3.84]	0.4013 [2.24]	0.9685 [3.78]
		Abaqus	0.3324	0.6457	1.5510	0.2056	0.3925	0.9332
SFSF	Al_2O_3	Present	0.1600 [0.88]	1.5943 [0.69]	0.7834 [1.05]	0.1356 [1.80]	1.3485 [1.88]	0.6625 [2.20]
		Abaqus	0.1586	1.5833	0.7752	0.1332	1.3236	0.6482
	0.5	Present	0.2292	1.7403	1.4440	0.1819	1.3600	1.1282
	5	Present	0.3809	1.0655	2.8290	0.2657	0.7098	1.8841
	Al	Present	0.5568 [2.67]	1.0081 [2.19]	2.6883 [2.83]	0.3471 [3.85]	0.6175 [3.17]	1.6465 [4.34]
		Abaqus	0.5423	0.9864	2.6143	0.3342	0.5985	1.5779
SSSC	Al_2O_3	Present	0.0357 [0.83]	0.4391 [3.47]	0.1509 [0.59]	0.0304 [0.33]	0.3714 [2.41]	0.1276 [1.10]
		Abaqus	0.0360	0.4549	0.1518	0.0303	0.3806	0.1262
	0.5	Present	0.0510	0.4798	0.2784	0.0408	0.3746	0.2174
	5	Present	0.0868	0.2929	0.5439	0.0614	0.1947	0.3613
	Al	Present	0.1267 [0.63]	0.2764 [4.12]	0.5153 [0.31]	0.0810 [1.37]	0.1698 [4.87]	0.3140 [1.78]
		Abaqus	0.1259	0.2883	0.5137	0.0799	0.1785	0.3085
SCSC	Al_2O_3	Present	0.0254 [2.30]	0.3152 [6.60]	0.0979 [3.73]	0.0217 [1.80]	0.2665 [5.70]	0.0827 [1.89]
		Abaqus	0.0260	0.3375	0.1017	0.0221	0.2826	0.0843
	0.5	Present	0.0362	0.3445	0.1808	0.0290	0.2688	0.1410
	5	Present	0.0625	0.2100	0.3521	0.0446	0.1393	0.2333
	Al	Present	0.0911 [1.61]	0.2020 [6.70]	0.3328 [4.20]	0.0590 [1.66]	0.1269 [6.62]	0.2018 [3.67]
		Abaqus	0.0926	0.2165	0.3474	0.0600	0.1359	0.2095
SSSS	Al_2O_3	Present	0.0509 [1.39]	0.6218 [0.01]	0.2291 [2.96]	0.0433 [2.85]	0.5259 [1.34]	0.1937 [4.81]
		Abaqus	0.0502	0.6217	0.2225	0.0421	0.5189	0.1848
	0.5	Present	0.0728	0.6791	0.4225	0.0580	0.5305	0.3301
	5	Present	0.1225	0.4152	0.8269	0.0862	0.2763	0.5502
	Al	Present	0.1790 [3.46]	0.3923 [0.82]	0.7847 [5.41]	0.1132 [5.10]	0.2397 [1.09]	0.4795 [6.08]
		Abaqus	0.1730	0.3891	0.7444	0.1077	0.2371	0.4520

*$[\%Error] = \left|\frac{state\ space\ result - Abaqus\ result}{Abaqus\ result}\right| \times 100$

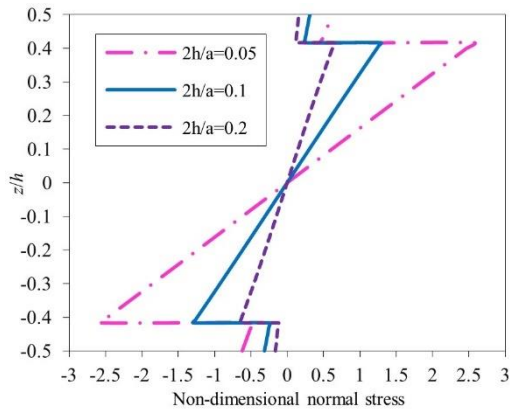

Fig. 3 Variation of non-dimensional normal stress ($\bar{\sigma}_x$) through the smart transversely isotropic plate thickness with different thickness-to-side ratios

(BCs: SSSS, $h_p/2h$ =0.1).

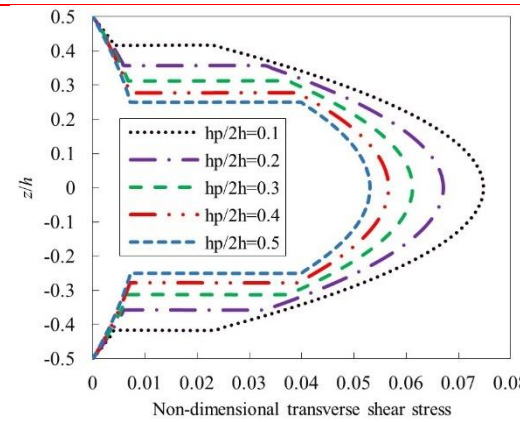

Fig. 4 Variation of non-dimensional transverse shear stress ($\bar{\tau}_{xz}$) through the smart transversely isotropic plate thickness with different piezoelectric thickness ratios (BCs: SSSC, a/b =1, $2h$/a =0.1).

Figs. 5-6 are plotted to show the validation of the non-dimensional deflection with the results reported by Mohammadimehr *et al.* (2015). In this reference, the bending analysis of a fully simply supported smart FG plate under short-circuited conditions was investigated using the third-order shear deformation theory and Navier's solution. As seen, there is a good agreement between the results. Fig. 5 depicts the effect of the power-law index on the distribution of non-dimensional deflection across the length of a smart FG plate. The plot demonstrates that an increase in the power-law index leads to a corresponding increase in transverse deflection, primarily due to the lower elastic modulus of Al in comparison to Al_2O_3. The results also reveal that increasing the power-law index reduces the stiffness of the core plate due to the higher volume fraction of Al. Fig. 6 presents the influence of piezoelectric layer thickness on the non-dimensional deflection, considering different power-law indices. The plot shows that deflection values decrease as the thickness of the piezoelectric layers increases. This trend can be attributed to the higher plate stiffness and more substantial electromechanical coupling effects of thicker piezoelectric layers. Additionally, the study finds that the deflection values increase as the power-law index increases and the plate stiffness decreases due to the lower elastic modulus of Al compared to Al2O3.

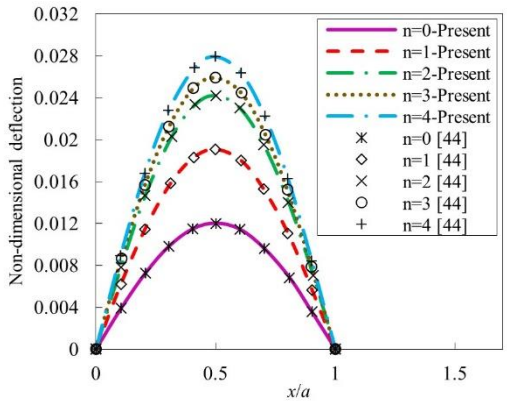

Fig. 5 Comparison of non-dimensional deflection ($\overline{W}$) of smart FG plate considering different power-law indices (BCs.: SSSS, a=b=400mm, h=2.5 mm, hp=1, q_0=100 N/m2).

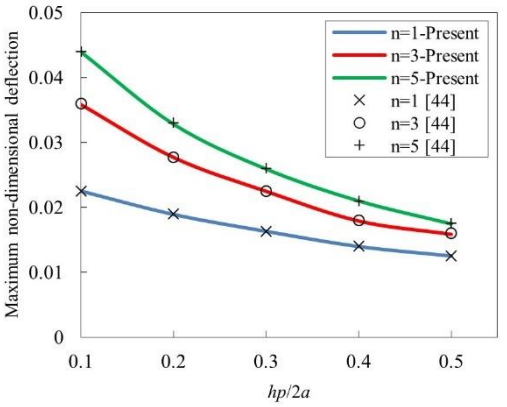

Fig. 6 Comparison of non-dimensional deflection ($\overline{W}$) of smart FG plate considering different power-law indices (BCs: SSSS, a=b=400mm, h=2.5 mm, q_0=100 N/m2).

Fig. 7 shows the non-dimensional normal stress distribution over the plate thickness under different boundary conditions. There are slight differences between the simulation results and the present study's outcomes. For all boundary conditions, the non-dimensional normal stress has its highest value at the interface between the core and piezoelectric layers, and plates with SFSF and SCSC boundary conditions have the largest and smallest normal stresses, respectively.

Fig. 8 displays the distribution of non-dimensional transverse deflection ($\bar{W}$) through the width of the smart FG plate with different boundary conditions. As observed, the maximum deflection occurs at different y coordinates depending on the boundary condition.

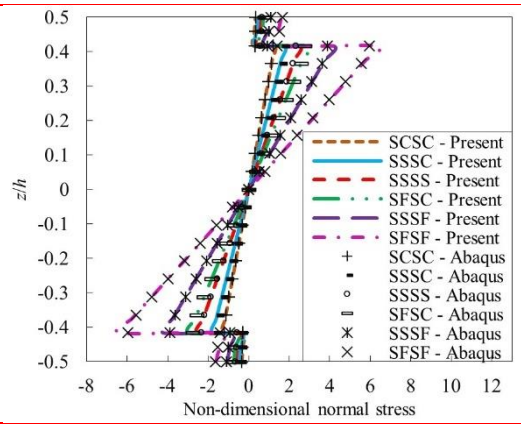

Fig. 7 Comparison of non-dimensional normal stress ($\bar{\sigma}_x$) distribution with Abaqus results considering different boundary conditions (n=0, $2h/a$=0.05, a/b =1, $h_p/2h$=0.1).

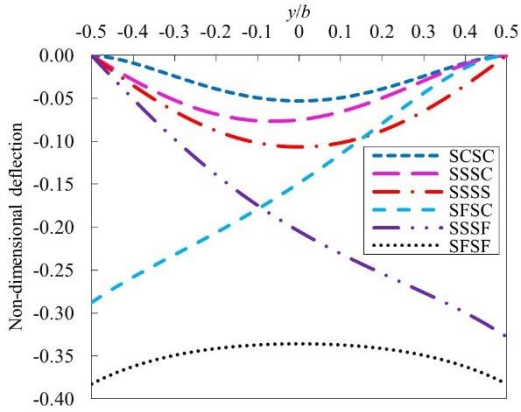

Fig. 8 Distribution of non-dimensional deflection ($\bar{W}(a/2, y, 0)$) of smart FG plate through the plate width considering different boundary conditions (n=2, $2h/a$=0.1, a/b =1, $h_p/2h$ =0.1).

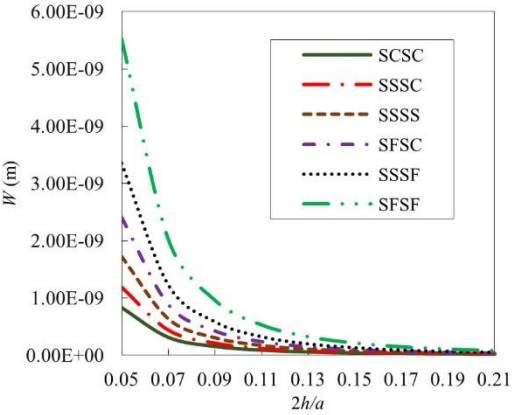

Fig. 9. Central deflection of the smart FG plate versus thickness-to-side ratio considering different boundary conditions (a=b=1m, q_0=1N, n=2, $hp/2h$ =0.1).

A plot of the thickness-to-side ratio ($2h/a$) vs the center transverse deflection of the smart FG plate under various boundary circumstances is shown in Fig. 9. As expected, for all boundary conditions increasing the thickness-to-side ratio leads to a reduction in deflection due to a higher amount of stiffness of thicker plates. Additionally, plates with SCSC and SFSF boundary conditions have the highest and lowest stiffness values, respectively, for a given value of the thickness-to-side ratio. Consequently, they have the lowest and highest value for deflection, respectively.

5. Conclusions

The current study offers an analytical solution for the bending problem involving a rectangular FG plate sandwiched between two piezoelectric layers and exposed to a uniformly distributed external force. This analytical solution is based on the four-variable refined plate theory. The plate has two simply supported edges opposite to one another, while two other edges may be arbitrarily exposed to supported, free, and clamped boundary conditions. Levy's solution and the state-space concept are employed to solve the structure's underlying equations. Comparing this article's results with the available data and the results from the Abaqus simulations confirms that the plate theory used, and the accompanying solution approach are highly accurate and efficient. Additionally, the influence of various parameters on the outcomes has been looked at, and the following findings have been drawn:

- As a capability of the refined plate theory, a parabolic variation was estimated for transverse shear stresses across the plate thickness.
- As the thickness of the core layer increases due to higher amounts of plate stiffness, the corresponding deflection, normal stress, and shear stress values will decrease.
- Increasing the piezoelectric layer thickness causes the values of normal and shear stresses to decrease due to the higher amount of plate stiffness and stronger electromechanical coupling effects of thicker piezoelectric layers.
- Having more constraints at the plate boundaries increases the structure stiffness resulting in a reduction in deflection, normal stress, and shear stress values.
- Since Al has a lower modulus of elasticity than Al_2O_3, lowering the power-law index results in a lower value for plate stiffness. Consequently, the deflection's value will rise.

Declaration of Competing Interest

The authors declare that they have no known competing financial interests or personal relationships that could have appeared to influence the work reported in this paper.

Availability of data and material:

The data presented in this study are available on request from the corresponding author. The data are not publicly available because it also forms part of an ongoing study.

Appendix A:

The matrix components of a transversely isotropic piezoelectric layer and for an FG core plate are defined as:

$$\bar{C}_{11} = C_{11} - \frac{C_{13}^2}{C_{33}}, \qquad \bar{C}_{12} = C_{12} - \frac{C_{13}^2}{C_{33}},$$
$$\bar{e}_{31} = e_{31} - \frac{C_{13}}{C_{33}} e_{33}, \qquad \bar{\eta}_{33} = \eta_{33} + \frac{e_{33}^2}{C_{33}}$$
$$Q_{11} = \frac{E(z)}{1-\upsilon^2}, \quad Q_{12} = \frac{\upsilon E(z)}{(1-\upsilon^2)}, \quad Q_{66} = \frac{E(z)}{2(1+\upsilon)} \tag{A1}$$

The matrix components of Eq. (21) are defined as:

$$\boldsymbol{N} = \{N_x, N_y, N_{xy}\}^T, \quad \boldsymbol{M}^b = \{M_x^b, M_y^b, M_{xy}^b\}^T$$
$$\boldsymbol{M}^s = \{M_x^s, M_y^s, M_{xy}^s\}^T, \quad 0 = \{0,0,0\}^T,$$
$$\boldsymbol{K} = \{\mu_1, \mu_1, 0\}^T, \quad \boldsymbol{T} = \{\mu_2, \mu_2, 0\}^T, \boldsymbol{S} = \{S_{yz}, S_{xz}\}^T \tag{A2}$$
$$\boldsymbol{\varepsilon} = \left\{\frac{\partial u_0}{\partial x}, \frac{\partial v_0}{\partial y}, \frac{\partial u_0}{\partial y} + \frac{\partial v_0}{\partial x}\right\}^T,$$

$$\boldsymbol{\kappa}^b = \left\{-\frac{\partial^2 w_b}{\partial x^2}, -\frac{\partial^2 w_b}{\partial y^2}, -2\frac{\partial^2 w_b}{\partial x \partial y}\right\}^T$$
$$\boldsymbol{\kappa}^s = \left\{-\frac{\partial^2 w_s}{\partial x^2}, -\frac{\partial^2 w_s}{\partial y^2}, -\frac{2\partial^2 w_s}{\partial x \partial y}\right\}^T, \tag{A2}$$
$$\boldsymbol{\gamma} = \left\{\frac{\partial w_s}{\partial y}, \frac{\partial w_s}{\partial x}\right\}^T, \qquad \boldsymbol{\Gamma} = \left\{\frac{\partial \varphi}{\partial y}, \frac{\partial \varphi}{\partial x}\right\}^T$$

And

$$\boldsymbol{A} = \begin{bmatrix} A_{11} & A_{12} & 0 \\ A_{12} & A_{22} & 0 \\ 0 & 0 & A_{66} \end{bmatrix}, \qquad \boldsymbol{B} = \begin{bmatrix} B_{11} & B_{12} & 0 \\ B_{12} & B_{22} & 0 \\ 0 & 0 & B_{66} \end{bmatrix},$$
$$\boldsymbol{D} = \begin{bmatrix} D_{11} & D_{12} & 0 \\ D_{12} & D_{22} & 0 \\ 0 & 0 & D_{66} \end{bmatrix}, \qquad \boldsymbol{H} = \begin{bmatrix} H_{11} & H_{12} & 0 \\ H_{12} & H_{22} & 0 \\ 0 & 0 & H_{66} \end{bmatrix}, \tag{A3}$$
$$\boldsymbol{B}^s = \begin{bmatrix} B_{11}^s & B_{12}^s & 0 \\ B_{12}^s & B_{22}^s & 0 \\ 0 & 0 & B_{66}^s \end{bmatrix}, \qquad \boldsymbol{D}^s = \begin{bmatrix} D_{11}^s & D_{12}^s & 0 \\ D_{12}^s & D_{22}^s & 0 \\ 0 & 0 & D_{66}^s \end{bmatrix},$$
$$\boldsymbol{A}^s = \begin{bmatrix} A_{11}^s & 0 \\ 0 & A_{11}^s \end{bmatrix}$$

in which A_{ij}, B_{ij}, etc. are the rigidity matrix components, defined by:

$$\begin{Bmatrix} A_{1i} \\ B_{1i} \\ B_{1i}^s \\ D_{1i} \\ D_{1i}^s \\ H_{1i} \end{Bmatrix} = \int_{-h-h_p}^{-h} \bar{C}_{1i} \begin{Bmatrix} 1 \\ z \\ f \\ z^2 \\ zf \\ f^2 \end{Bmatrix} dz + \int_{-h}^{h} Q_{1i} \begin{Bmatrix} 1 \\ z \\ f \\ z^2 \\ zf \\ f^2 \end{Bmatrix} dz + \int_{h}^{h+h_p} \bar{C}_{1i} \begin{Bmatrix} 1 \\ z \\ f \\ z^2 \\ zf \\ f^2 \end{Bmatrix} dz \quad , i = 1,2$$

$$\begin{Bmatrix} A_{66} \\ B_{66} \\ B_{66}^s \\ D_{66} \\ D_{66}^s \\ H_{66} \end{Bmatrix} = \int_{-h-h_p}^{-h} \frac{1}{2}(\bar{C}_{11} - \bar{C}_{12}) \begin{Bmatrix} 1 \\ z \\ f \\ z^2 \\ zf \\ f^2 \end{Bmatrix} dz + \int_{-h}^{h} Q_{66} \begin{Bmatrix} 1 \\ z \\ f \\ z^2 \\ zf \\ f^2 \end{Bmatrix} dz + \int_{h}^{h+h_p} \frac{1}{2}(\bar{C}_{11} - \bar{C}_{12}) \begin{Bmatrix} 1 \\ z \\ f \\ z^2 \\ zf \\ f^2 \end{Bmatrix} dz \tag{A4}$$

$$(A_{22}, B_{22}, B_{22}^s, D_{22}, D_{22}^s, H_{22}) = (A_{11}, B_{11}, B_{11}^s, D_{11}, D_{11}^s, H_{11})$$

$$A_{11}^s = \int_{-h-h_p}^{-h} C_{55} g^2 \, dz + \int_{-h}^{h} Q_{66} g^2 dz + \int_{h}^{h+h_p} C_{55} g^2 \, dz$$

The coefficients μ_i of Eqs. (22) are defined as:

$$\mu_1 = \frac{4}{3} e_{31} h_p, \qquad \mu_2 = \frac{1}{6} \frac{h_p(8h^2 + 6hh_p + h_p^2)}{(h+h_p)^2} e_{31}, \qquad \mu_3 = -\frac{1}{6} \frac{h_p^2(10h + 7h_p)}{(h+h_p)^2} e_{51} \tag{A5}$$

The coefficients Υ_i of Eq. (24) are defined as:

$$\Upsilon_1 = -\frac{\left(\frac{e_{31} - 5e_{51}}{3}\right) h_p^3 - \frac{h(5e_{51} - 3e_{31})h_p^2}{2} + 2e_{31}h^2 h_p}{(h+h_p)^2}, \qquad \Upsilon_2 = \frac{4}{3}\eta_{11} h_p, \qquad \Upsilon_3 = 2e_{31} h_p, \qquad \Upsilon_4 = \frac{16\eta_{33}}{h_p} \tag{A6}$$

Appendix B:

Boundary conditions at $y=b/2$ and $y=-b/2$ for simply supported, clamped or free are taken as follows:

- Simply supported

$$u_0 = w_b = w_s = N_y = M_y^b = M_y^s = \varphi = 0 \quad \text{(B1)}$$

- Clamped

$$u_0 = v_0 = w_b = w_s = \frac{\partial w_b}{\partial y} = \frac{\partial w_s}{\partial y} = \varphi = 0 \quad \text{(B2)}$$

- Free

$$N_y = N_{xy} = M_y^b = M_y^s = \varphi = \frac{\partial M_y^b}{\partial y} + \frac{2\partial M_{xy}^b}{\partial x} = \frac{\partial M_y^s}{\partial y} + 2\frac{\partial M_{xy}^s}{\partial x} + S_{yz} = 0 \quad \text{(B3)}$$

c_i, c_{ij} and c_{ijm} constants in Eqs. (30) are described as:

$$c_1 = \frac{A_{11}\alpha^2}{A_{66}}, c_2 = \frac{-(A_{12}+A_{66})\alpha}{A_{66}}, c_3 = \frac{-B_{11}\alpha^3}{A_{66}}, c_{3s} = \frac{-B_{11}^s\alpha^3}{A_{66}}, c_4 = \frac{(B_{12}+2B_{66})\alpha}{A_{66}}, c_{4s} = \frac{(B_{12}^s+2B_{66}^s)\alpha}{A_{66}},$$

$$c_5 = \frac{(A_{12}+A_{66})\alpha}{A_{22}}, c_6 = \frac{(A_{66}\alpha^2)}{A_{22}}, c_7 = \frac{-(B_{12}+2B_{66})\alpha^2}{A_{22}}, c_{7s} = \frac{-(B_{12}^s+2B_{66}^s)\alpha^2}{A_{22}}, c_8 = \frac{B_{22}}{A_{22}}, c_{8s} = \frac{B_{22}^s}{A_{22}}$$

$$c_{11m} = \frac{\Upsilon_3\alpha^2}{\Upsilon_2}, c_{12m} = \frac{-\Upsilon_3}{\Upsilon_2}, c_{13m} = \frac{-\Upsilon_1\alpha^2}{\Upsilon_2}, c_{14m} = \frac{\Upsilon_1}{\Upsilon_2}, c_{16m} = \frac{(\Upsilon_2\alpha^2+\Upsilon_4)}{\Upsilon_2}, c_{9s} = \frac{(B_{11}^s\alpha^3+c_1\delta+p_1\hbar)}{\lambda}$$

$$c_{15s} = \frac{(1+p_8\hbar)}{\lambda}, c_{16s} = \frac{\left((c_{17m}-\alpha^2)(\mu_3-\mu_2)+p_7\hbar\right)}{\lambda}, c_{10s} = \frac{(B_{22}^s c_6 + c_2\delta - (B_{12}^s+2B_{66}^s)\alpha^2 + p_2\hbar)}{\lambda}$$

$$c_{11s} = \frac{(c_3\delta - D_{11}^s\alpha^4 + c_{11m}(\mu_3-\mu_2)+p_3\hbar)}{\lambda}, c_9 = (p_1+c_{9s}p_9), c_{10} = (p_2+c_{10s}p_9), c_{11} = (p_3+c_{11s}p_9) \quad \text{(B4)}$$

$$c_{12} = (p_4+c_{12s}p_9), c_{13} = (p_5+c_{13s}p_9), c_{14} = (p_6+c_{14s}p_9), c_{15} = (p_8+c_{15s}p_9), c_{16} = (p_7+c_{16s}p_9)$$

$$c_{12s} = \frac{(B_{22}^s c_7 + c_4\delta + 2(D_{12}^s+2D_{66}^s)\alpha^2 + c_{12m}(\mu_3-\mu_2)+p_4\hbar)}{\lambda}$$

$$c_{13s} = \frac{(c_{3s}\delta - H_{11}\alpha^4 - A_{11}^s\alpha^2 + c_{13m}(\mu_3-\mu_2)+p_5\hbar)}{\lambda}$$

$$c_{14s} = \frac{(B_{22}^s c_{7s} + c_{4s}\delta + 2(H_{12}+2H_{66})\alpha^2 + A_{11}^s + c_{14m}(\mu_3-\mu_2)+p_6\hbar)}{\lambda}$$

and

$$p_1 = \frac{(B_{11}\alpha^3+c_1\psi)}{\chi}, p_2 = \frac{(B_{22}c_6+c_2\psi-(B_{12}+2B_{66})\alpha^2)}{\chi}, p_3 = \frac{(c_3\psi - D_{11}\alpha^4 - \mu_1 c_{11m})}{\chi}$$

$$p_4 = \frac{(B_{22}c_7+c_4\psi+2(D_{12}+2D_{66})\alpha^2 - \mu_1 c_{12m})}{\chi}, p_5 = \frac{(c_{3s}\psi - D_{11}^s\alpha^4 - \mu_1 c_{13m})}{\chi}$$

$$p_6 = \frac{(B_{22}c_{7s}+c_{4s}\psi+2(D_{12}^s+2D_{66}^s)\alpha^2 - \mu_1 c_{14m})}{\chi}, p_7 = \frac{(\mu_1\alpha^2 - \mu_1 c_{16m})}{\chi}, p_8 = \frac{1}{\chi} \quad \text{(B5)}$$

$$p_9 = \frac{(c_{8s}B_{22} - D_{22}^s)}{\chi}, \delta = (B_{22}^s c_5 - (B_{12}^s+2B_{66}^s)\alpha), \lambda = H_{22} - B_{22}^s c_{8s} - p_9(B_{22}^s c_8 - D_{22}^s)$$

$$\hbar = B_{22}^s c_8 - D_{22}^s, \qquad \psi = (B_{22}c_5 - (B_{12}+2B_{66})\alpha), \qquad \chi = D_{22} - c_8 B_{22}$$

Also, different boundary conditions can be written in terms of $(U_m(y),\ V_m(y),\ W_{bm}(y),\ W_{sm}(y)$ and $\varphi_m(y))$ as follows:

- Simply supported:

$$U_m(y) = W_{bm}(y) = W_{sm}(y) = \varphi_m(y) = 0$$
$$-A_{12}\alpha U_m(y) + B_{12}\alpha^2 W_{bm}(y) + B_{12}^s\alpha^2 W_{sm}(y) + A_{22}V_m'(y) - B_{22}W_{bm}''(y) - B_{22}^s W_{sm}''(y) = 0$$
$$-B_{12}\alpha U_m(y) + D_{12}\alpha^2 W_{bm}(y) + D_{12}^s\alpha^2 W_{sm}(y) + B_{22}V_m'(y) - D_{22}W_{bm}''(y) - D_{22}^s W_{sm}''(y) - \mu_1\varphi_m(y) = 0 \quad \text{(B6)}$$
$$-B_{12}^s\alpha U_m(y) + D_{12}^s\alpha^2 W_{bm}(y) + H_{12}\alpha^2 W_{sm}(y) + B_{22}^s V_m'(y) - D_{22}^s W_{bm}''(y) - H_{22}W_{sm}''(y) - \mu_2\varphi_m(y) = 0$$

- Clamped:

$$U_m(y) = V_m(y) = W_{bm}(y) = W_{sm}(y) = W_{bm}'(y) = W_{sm}'(y) = \varphi_m(y) = 0 \quad \text{(B7)}$$

- Free:

$$\varphi_m = 0$$
$$-A_{12}\alpha U_m(y) + B_{12}\alpha^2 W_{bm}(y) + B_{12}^s\alpha^2 W_{sm}(y) + A_{22}V_m'(y) - B_{22}W_{bm}''(y) - B_{22}^s W_{sm}''(y) = 0$$
$$A_{66}(U_m'(y) + \alpha V_m(y)) - 2B_{66}\alpha W_{bm}'(y) - 2B_{66}^s\alpha W_{sm}'(y) = 0$$
$$-B_{12}\alpha U_m(y) + D_{12}\alpha^2 W_{bm}(y) + D_{12}^s\alpha^2 W_{sm}(y) + B_{22}V_m'(y) - D_{22}W_{bm}''(y) - D_{22}^s W_{sm}''(y) - \mu_1\varphi_m(y) = 0$$
$$-B_{12}^s\alpha U_m(y) + D_{12}^s\alpha^2 W_{bm}(y) + H_{12}\alpha^2 W_{sm}(y) + B_{22}^s V_m'(y) - D_{22}^s W_{bm}''(y) - H_{22}W_{sm}''(y) = 0 \quad \text{(B8)}$$
$$(B_{22}c_5 - B_{12}\alpha - 2B_{66}\alpha)U_m'(y) + (B_{22}c_6 - 2B_{66}\alpha^2)V_m(y) + (B_{22}c_7 + D_{12}\alpha^2 + 4D_{66}\alpha^2)W_{bm}'(y) + (B_{22}c_{7s} + D_{12}^s\alpha^2 + 4D_{66}^s\alpha^2)W_{sm}'(y) + (B_{22}c_8 - D_{22})W_{bm}'''(y) + (B_{22}c_{8s} - D_{22}^s)W_{sm}'''(y) - \mu_1\varphi_m'(y) = 0$$
$$(B_{22}^s c_5 - B_{12}^s\alpha - 2B_{66}^s\alpha)U_m'(y) + (B_{22}^s c_6 - 2B_{66}^s\alpha^2)V_m(y) + (B_{22}^s c_7 + D_{12}^s\alpha^2 + 4D_{66}^s\alpha^2)W_{bm}'(y) + (B_{22}^s c_{7s} + H_{12}\alpha^2 + 4H_{66}\alpha^2 + A_{11}^s)W_{sm}'(y) + (B_{22}^s c_8 - D_{22}^s)W_{bm}'''(y) + (B_{22}^s c_{8s} - H_{22})W_{sm}'''(y) + \mu_3\varphi_m'(y) = 0$$

References

Abad, F., and Rouzegar, J. (2017), "An exact spectral element method for free vibration analysis of FG plate integrated with piezoelectric layers", Composite Structures, **180**: 696-708.

Abad, F., and Rouzegar, J. (2019), "Exact wave propagation analysis of moderately thick Levy-type plate with piezoelectric layers using spectral element method", Thin-Walled Structures, **141**: 319-31.

Abad, F., Rouzegar, J., and Lotfian, S. (2023), "Application of the exact spectral element method in the analysis of the smart functionally graded plate", Steel and Composite Structures, An International Journal, **47**: 297-313.

Abbaspour, F., and Arvin, H. (2021), "Buckling treatment of piezoelectric functionally graded graphene platelets micro plates", Steel and Composite Structures, An International Journal, **38**: 337-53.

Arefi, M., Pourjamshidian, M., and Arani, A.G. (2019), "Dynamic instability region analysis of sandwich piezoelectric nano-beam with FG-CNTRCs face-sheets based on various high-order shear deformation and nonlocal strain gradient theory", Steel and Composite Structures, An International Journal, **32**: 157-71.

Arefi, M., Soltan Arani, AH. (2020), "Nonlocal vibration analysis of the three-layered FG nanoplates subjected to applied electric potential considering thickness stretching effect", Proceedings of the Institution of Mechanical Engineers, Part L: Journal of Materials: Design and Applications, **234**: 1183-202

Atmane, R.A., Mahmoudi, N., and Bennai, R. (2021), "Investigation on the dynamic response of porous FGM beams resting on variable foundation using a new higher order shear deformation theory", Steel and Composite Structures, An International Journal, **39**: 95-107.

Belabed, Z., Selim, M.M., Slimani, O., Taibi, N., Tounsi, A., and Hussain, M. (2021), "An efficient higher order shear deformation theory for free vibration analysis of functionally graded shells", Steel and Composite Structures, An International Journal, **40**: 307-21.

Boukhlif, Z. (2019), "A simple quasi-3D HSDT for the dynamics analysis of FG thick plate on elastic foundation", Steel and Composite Structures, An International Journal, **31**: 503-16.

Chan, D.Q., Quan, T.Q., Phi, B.G., Van Hieu, D., Duc, N.D. (2022) "Buckling analysis and dynamic response of FGM sandwich cylindrical panels in thermal environments using nonlocal strain gradient theory", Acta Mechanica, **233**: 2213-35.

Demirhan, P.A., and Taskin, V. (2017), "Levy solution for bending analysis of functionally graded sandwich plates based on four variable plate theory", Composite Structures, **177**: 80-95.

Demirhan, P.A., and Taskin, V. (2019), "Bending and free vibration analysis of Levy-type porous functionally graded plate using state space approach", Composites Part B: Engineering, **160**: 661-76.

Fourn, H., Atmane, H.A., Bourada, M., Bousahla, A.A., Tounsi, A., and Mahmoud, S.R. (2018), "A novel four variable refined plate theory for wave propagation in functionally graded material plates", Steel and Composite Structures, An International Journal, **27**: 109-22.

Franklin, J.N. (2012). Matrix Theory, Courier Corporation.

Guellil, M., Saidi, H., Bourada, F., Bousahla, A.A., Tounsi, A., Al-Zahrani, M.M., Hussain, M., and Mahmoud, S. (2021), "Influences of porosity distributions and boundary conditions on mechanical bending response of functionally graded plates resting on Pasternak foundation", Steel and Composite Structures, An International Journal, **38**: 1-15.

Hachemi, H., Bousahla, A.A., Kaci, A., Bourada, F., Tounsi, A., Benrahou, K.H., Tounsi, A., Al-Zahrani, M.M., and Mahmoud, S. (2021), "Bending analysis of functionally graded plates using a

new refined quasi-3D shear deformation theory and the concept of the neutral surface position", Steel and Composite Structures, An International Journal, **39**: 51-64.

Huang, W., and Tahouneh, V. (2021), "Frequency study of porous FGPM beam on two-parameter elastic foundations via Timoshenko theory", Steel and Composite Structures, An International Journal, **40**: 139-56.

Huang, Y., Li, Y., Zhang, L., Zhang, H., and Gao, Y. (2020), "Dynamic analysis of a multilayered piezoelectric two-dimensional quasicrystal cylindrical shell filled with compressible fluid using the state-space approach", Acta Mechanica, **231**: 2351-68.

Kouider, D., Kaci, A., Selim, M.M., Bousahla, A.A., Bourada, F., Tounsi, A., Tounsi, A., and Hussain, M. (2021), "An original four-variable quasi-3D shear deformation theory for the static and free vibration analysis of new type of sandwich plates with both FG face sheets and FGM hard core", Steel and Composite Structures, An International Journal, **41**: 167-91.

Lee, J.S., and Jiang, L.Z. (1996), "Exact electroelastic analysis of piezoelectric laminae via state space approach", International Journal of Solids and Structures, **33**: 977-90.

Liu, X., Wang, Y., Wang, G., Yang, B., and Xu, R. (2022), "Dynamic analysis of RC beams externally bonded with FRP plates using state space method", Engineering Structures, **253**: 113788.https://doi.org/10.1016/j.engstruct.2021.113788

Mahamood, R.M., and Akinlabi, E.T. (2017), Types of Functionally Graded Materials and Their Areas of Application. (Rasheedat Modupe Mahamood and Esther Titilayo Akinlabi), Functionally Graded Materials, Springer International Publishing: Cham.

Menasria, A., Kaci, A., Bousahla, A.A., Bourada, F., Tounsi, A., Benrahou, K.H., Tounsi, A., Bedia, E.A., and Mahmoud, S. (2020), "A four-unknown refined plate theory for dynamic analysis of FG-sandwich plates under various boundary conditions", Steel and Composite Structures, An International Journal, **36**: 355-67.

Mohammadimehr, M., rostami, and Arefi, M. (2015), "Electro-elastic analysis of a sandwich thick plate considering FG core and composite piezoelectric layers on Pasternak foundation using TSDT", Steel and Composite Structures, An International Journal.10.12989/scs.2016.20.3.513

Pham, Q.-H., Nguyen, P.-C., Tran, V.-K., and Nguyen-Thoi, T. (2021), "Finite element analysis for functionally graded porous nano-plates resting on elastic foundation", Steel and Composite Structures, An International Journal, **41**: 149-66.

Rahimi, Z., Sumelka, W., Shafiei, S. (2018), "The analysis of non-linear free vibration of FGM nano-beams based on the conformable fractional non-local model. Bulletin of the Polish Academy of Sciences", Technical Sciences, **66**: 737-45.

Razgordanisharahi, A., Alipour Ghassabi, A., and Hellmich, C. (2023), "Free vibration analysis of cylindrical honeycomb sandwich panels using state-space Levy method", Thin-Walled Structures, **182**: 110308. https://doi.org/10.1016/j.tws.2022.110308

Rouzegar, J., and Abad, F. (2015), "Free vibration analysis of FG plate with piezoelectric layers using four-variable refined plate theory", Thin-Walled Structures, **89**: 76-83.

Rouzegar, J., Koohpeima, R., and Abad, F. (2020), "Dynamic Analysis of Laminated Composite Plate Integrated with a Piezoelectric Actuator Using Four-Variable Refined Plate Theory", Iranian Journal of Science and Technology, Transactions of Mechanical Engineering, **44**: 557-70.10.1007/s40997-019-00284-1

Rouzegar, J., Salmanpour, N., Abad, F., Li, L. (2022) "An analytical state-space solution for free vibration of sandwich piezoelectric plate with functionally graded core", Scientia Iranica, **29**: 502-33.

Stempin, P., Sumelka, W. (2021) "Formulation and experimental validation of space-fractional Timoshenko beam model with functionally graded materials effects", Computational Mechanics, **68**: 697-708

Thai, H.-T., and Choi, D.-H. (2013a), "Analytical solutions of refined plate theory for bending, buckling and vibration analyses of thick plates", Applied Mathematical Modelling, **37**: 8310-23.

Thai, H.-T., and Choi, D.-H. (2013b), "Efficient higher-order shear deformation theories for bending and free vibration analyses of functionally graded plates", Archive of Applied Mechanics, **83**: 1755-71.10.1007/s00419-013-0776-z

Thai, H.-T., and Choi, D.-H. (2013c), "Finite element formulation of various four unknown shear deformation theories for functionally graded plates", Finite Elements in Analysis and Design, **75**: 50-61.https://doi.org/10.1016/j.finel.2013.07.003

Thai, H.-T., Park, M., and Choi, D.-H. (2013), "A simple refined theory for bending, buckling, and vibration of thick plates resting on elastic foundation", International Journal of Mechanical Sciences, **73**: 40-52.

Tiersten, H.F. (2013). Linear piezoelectric plate vibrations: Elements of the linear theory of piezoelectricity and the vibrations piezoelectric plates, Springer.

Wang, Q., Quek, S., Sun, C., and Liu, X. (2001), "Analysis of piezoelectric coupled circular plate", Smart Mater Struct, **10**: 229.

Zarga, D. (2019), "Thermomechanical bending study for functionally graded sandwich plates using a simple quasi-3D shear deformation theory", Steel and Composite Structures, An International Journal, **32**: 389-410.

Zenkour, A.M. (2006), "Generalized shear deformation theory for bending analysis of functionally graded plates", Applied Mathematical Modelling, **30**: 67-84.

Zenkour, A.M., Radwan, A.F. (2020) "Bending and buckling analysis of FGM plates resting on elastic foundations in hygrothermal environment", Archives of Civil and Mechanical Engineering, **20**: 112.

Zhou, Y., Nyberg, T., Xiong, G., and Li, S. (2020), "State space finite element analysis for piezoelectric laminated curved beam with variable curvature", Mechanics of Advanced Materials and Structures, **27**: 265-73.